The molecular structure of melts along the carbonatite–kimberlite–basalt compositional joint: CO2and polymerisation

Yves Moussallam, Pierre Florian, Dario Corradini, Yann Morizet, Nicolas Sator, Rodolphe Vuilleumier, Bertrand Guillot, Giada Iacono Marziano, Burkhard C. Schmidt, Fabrice Gaillard

The molecular structure of melts along the carbonatite–kimberlite–basalt compositional joint: CO_2 and polymerisation

Yves Moussallam, Pierre Florian, Dario Corradini, Yann Morizet, Nicolas Sator, Vuilleumier, Bertrand Guillot, Giada Iacono-Marziano, Burkhard C. Schmidt, Fabrice Gaillard

Abstract

Transitional melts, intermediate in composition between silicate and carbonate melts, form by low degree partial melting of mantle peridotite and might be the most abundant type of melt in the asthenosphere. Their role in the transport of volatile elements and in metasomatic processes at the planetary scale might be significant yet they have remained largely unstudied. Their molecular structure has remained elusive in part because these melts are difficult to quench to glass. Here we use FTIR, Raman, ^{13}C and ^{29}Si NMR spectroscopy together with First Principle Molecular Dynamic (FPMD) simulations to investigate the molecular structure of transitional melts and in particular to assess the effect of CO_2 on their structure. We found that carbon in these glasses forms free ionic carbonate groups attracting cations away from their usual 'depolymerising' role in breaking up the covalent silicate network. Solution of CO_2 in these melts strongly modifies their structure resulting in a significant polymerisation of the aluminosilicate network with a decrease in NBO/Si of about 0.2 for every 5 mol% CO_2 dissolved.

This polymerisation effect is expected to influence the physical and transport properties of transitional melts. An increase in viscosity is expected with increasing CO_2 content, potentially leading to melt ponding at certain levels in the mantle such as at the lithosphere–asthenosphere boundary. Conversely an ascending and degassing transitional melt such as a kimberlite would become increasingly fluid during ascent hence potentially accelerate. Carbon-rich transitional melts are effectively composed of two sub-networks: a carbonate and a silicate one leading to peculiar physical and transport properties.

Keywords : CO_2; polymerisation; speciation; transitional melt; kimberlite; glass

1. Introduction

Carbon dioxide (CO_2) is typically the second-most abundant volatile in terrestrial melts. In common silicate melts, found near the Earth's surface and in its crust, its concentration is typically greatly inferior to that of water and its influence on the melt physical properties secondary. In the Earth's upper mantle however, carbon-rich and typically silica-poor melts, generated by low degree partial melting of the mantle are probably widespread (e.g. Wyllie and Huang, 1976, Eggler, 1978, Dalton and Presnall, 1998, Gudfinnsson and Presnall, 2005, Dasgupta and Hirschmann, 2006 and Dasgupta et al., 2013; Massuyeau et al., in press). Very low degree partial melting of carbonated peridotite at ~250 km depth produces carbonatite liquid (e.g. Dasgupta and Hirschmann, 2006). With either increasing temperature, decreasing pressure or with

Table 1
Starting oxide and natural rock powder mix compositions used for experiments (in wt%). The composition of a natural lamproite from Torre Alfina, Italy (Peccerillo et al., 1988), fused twice at 1400 °C and used to prepare the oxide-mix compositions is reported at the top of the table.

Name	SiO_2	TiO_2	Al_2O_3	FeO	MgO	CaO	Na_2O	K_2O	P_2O_5	CO_2	Total
TA	55.7	1.3	13.1	5.8	9.4	5.4	1.0	7.7	0.5	0.0	100
TA6	16.6	0.2	3.9	0.9	6.9	35.5	0.3	2.3	0.1	33.5	100
TA9	23.1	0.3	5.4	1.5	8.3	30.2	0.4	3.2	0.1	27.5	100
TA10	23.8	0.4	5.5	1.6	8.3	29.7	0.4	3.3	0.1	27.0	100
TA11	30.2	0.6	7.0	2.4	8.5	24.8	0.5	4.1	0.2	21.6	100
TA12	37.7	0.8	8.8	3.4	8.8	19.1	0.6	5.2	0.3	15.2	100

the addition of CO_2 or H_2O, the liquid produced by peridotite partial melting will become increasingly SiO_2-rich, forming kimberlite, melilitite and eventually basalt (e.g. Wyllie and Huang, 1976; Eggler, 1978; Wyllie, 1989). These melts – carbonatite, kimberlite and melilitite – transitional between pure carbonatite and silicate liquids (~10 to ~40 wt% SiO_2), can contain up to several tens of weight percent of CO_2 (Brey and Green, 1976; Moussallam et al., 2014). Understanding the effect of CO_2 on the structure of these melts/glasses is therefore a cornerstone to predict their physical characteristics and transport properties.

The effect of CO_2 on melt polymerisation has remained unclear. Eggler (1978) suggested that the dissolution of CO_2 as carbonate ion (CO_3^{2-}) should result in melt polymerisation via the reaction:

$$CO_2 + 2Q^n(M^{m+}) \rightleftharpoons CO_3^{2-}(M^{m+}) + 2Q^{n+1} \quad (1)$$

Where Q^n denotes a silica tetrahedron linked by bridging O atoms to n adjacent tetrahedra ($n = 0$ correspond to an isolated SiO_4 tetrahedron, $n = 4$ correspond to a fully connected tetrahedron with four bridging oxygen), M^{m+} denotes a metal cation in network modifying or charge balancing role. In Eq. (1), the increase in polymerisation is denoted by the building of Si–O–Si bonds.

This depiction has gained popularity, being referred to as a largely admitted concept in review articles (e.g. Mysen, 2013, 2012) and books (e.g. Frost and Frost, 2013; Mysen and Richet, 2005). Solid evidence of the effect of CO_2 dissolution on the aluminosilicate network structure however has been lacking. Mysen and Virgo (1980a, 1980b) found that CO_2 depolymerises albite and anortite melts while polymerising diopside and $NaCaAlSi_2O_7$ melts. Konschak (2008) investigated the albite – diopside joint and found no effect of CO_2 on polymerisation from $Ab_{50}Di_{50}$ to $Ab_{75}Di_{25}$ but found that a slight depolymerisation is associated with the addition of CO_2 to $Ab_{90}Di_{10}$. As noted by Ni and Keppler (2013) these evidence are all based on very subtle differences in Raman spectra, which interpretation can be controversial. All these studies have focused on the incorporation mechanisms of CO_2 and its impacts on the molecular structure of silicate melts. Here we look at CO_2 in transitional melts, typically produced by very low-degree partial mantle melting and with silica content being about half of that of basalts.

The principal question we target in this study is: Does carbon dioxide influence the degree of polymerisation of transitional melts? We present results from the first Infrared, Raman and Nuclear Magnetic Resonance (NMR) spectroscopy investigation of transitional glasses and compare them with results from Ab-initio First Principle Molecular Dynamic simulations applied to melt conditions. We explore a compositional range from ~44 to 23 mol% SiO_2 (on a volatile-free basis) with 0 to 26 mol% CO_2. For all compositions investigated, we show that (1) CO_2 is present in the glass and in the melt dominantly as carbonate ion (2) the degree of polymerisation of the glass/melt increases with increasing CO_2 content. We conclude that the physical properties of transitional melts such as viscosity, electrical conductivity and sound velocity are expected to be greatly affected by their CO_2 content with implications regarding melt mobility in the upper mantle.

We note that polymerisation, in this manuscript is strictly defined as the process by which oxygen atoms are shared between silica (or alumina) tetrahedra and is expressed as the ratio of non-bridging oxygens to tetrahedral cations (NBO/T) or as the ratio of non-bridging oxygens per silicon (NBO/Si). We further note that the NBO/T ratio is only a calculated 'statistical average' and various combinations of Q species can give the same NBO/T. The NBO/T concept fails past NBO/T = 4 but Q units at greater values can still join up in isolated 'polymerised units'.

2. Methods

2.1. Experimental methodology

2.1.1. Starting material

Starting materials were produced by mixing powders from a natural lamproite from Torre Alfina, Italy (Peccerillo et al., 1988) with various amounts of synthetic powders of pure oxides (SiO_2, Al_2O_3, MgO, $CaCO_3$, Na_2CO_3, K_2CO_3) and natural dolomite. The strategy was to produce a series of progressively more silica and alumina poor compositions additionally low in iron in order for the final product to be analysable by NMR spectroscopy. The source of CO_2 in experiments was mainly $CaCO_3$. The Torre Alfina rock, was fused twice in air at 1400 °C and quenched to glass in order to ensure homogeneity and remove any volatile present. The composition of all mixtures used as starting materials is reported in Table 1.

2.1.2. HP-HT experiments

Experiments were performed in the pressure range 0.1 to 1500 MPa. High temperature experiments at 0.1 MPa were performed in a high-temperature furnace. The sample was contained in a Pt crucible and heated to 1500 °C for 30 min and then quenched to glass by complete immersion in cold water.

Experiments at high pressure were performed by Moussallam et al. (2014) in the pressure range 50 to 350 MPa at relatively constant temperature (1225 to 1270 °C) with no added water and under oxidised conditions ($\log f O_2 = FMQ + 3$). Experiments were performed in internally heated pressure vessels at the ISTO-CNRS laboratory in Orléans which can reach pressures of up to 400 MPa (±3 MPa) under controlled temperature up to 1300 °C (±5 °C) (see supplementary information).

Experiments at 1500 MPa and 1350 °C were performed in a piston-cylinder apparatus with in a 3/4 inch (1.9 cm) assemblies. Experimental charges consisted of natural anhydrous sample powder (30 mg) loaded in sealed gold–palladium (Au80Pd20) capsules (1 cm in length, 2.5 mm inner diameter and 2.9 mm outer diameter). The capsules were introduced in a talc–pyrex–graphite furnace assembly and surrounded by MgO. A B-type thermocouple was located at ~1 mm atop of the capsule and the run temperature should be considered as a minimum value. Uncertainties are of 10% in relative for pressure and of 15 °C for temperature. We used a modified perforated anvil through which cold water was circulated in order to maximise quenching rate (>200 °C s^{-1}).

A pure carbonate glass of composition $K_2Mg(CO_3)_2$ was synthesised in internally heated pressure vessel at 803 °C and 1083

bar under relatively oxidised conditions ($\log f O_2 = FMQ + 3$) with no added water. This composition was shown previously to be quenchable to carbonate glass without crystallisation (Ragone et al., 1966; Genge et al., 1995). The sample was enriched in ^{13}C by using K213CO3 (99% ^{13}C) as starting material. Drop quench at the end of the experiment resulted in pure carbonate glass as indicated by the lack of birefringence in polarisation microscopy.

2.2. Analytical techniques

2.2.1. Microbeam analyses

All experimental products were examined by optical microscope and scanning electronic microscope (SEM) to check for the presence of quench crystals. Electron microprobe analyses (EMPA) were performed on a Cameca SXFive at the ISTO-CNRS laboratory in Orléans. Glasses were analysed using an accelerating voltage of 15 kV, a beam current of 6 nA and a defocused beam of 10 µm with a count time of 10 s. Na was analysed first in order to minimise its loss during analyses. No K loss with time was observed at our operating conditions.

2.2.2. Infrared spectroscopy

Infrared spectra were collected using a Nicolet 6700 FTIR spectrometer attached to a Continuum microscope. We used a Globar internal IR source with a KBr beam splitter and a liquid nitrogen cooled MCT/A detector. The spectral resolution was set to 4 cm^{-1}, and spectra were accumulated for 128 scans. Background spectra were acquired by accumulating 256 scans and used to correct for background. Spectra were obtained directly on small glass fragments (unpolished) in transmission mode.

2.2.3. Micro-Raman spectroscopy

An Innova 300-5W Argon ion laser (Coherent©) operating at 514 nm was used as the exciting source to produce Raman scattering. Spectra were collected by a Jobin–Yvon Labram spectrometer (focal distance = 300 mm) equipped with a grating with 2400 grooves/mm and a CCD detector. The spectral frequency position was calibrated using the emission lines of Ne- and Hg-lamps with an accuracy within ±1 cm^{-1}. Analyses were performed in confocal mode (hole = 500 µm, slit = 200 µm) and using a ×50 Olympus objective resulting in an analysed volume of a few μm^3. Spectra were acquired in the 700–1300 cm^{-1} spectral region which corresponds to the vibrational region for aluminosilicate framework symmetric stretch (ν_1 for Q^n species; e.g. Mysen et al., 1982) and also the symmetric stretch for CO_3^{2-} molecular groups (ν_1 for CO_3^{2-}) at around 1080 cm^{-1}. The acquisition time was of 10 × 60 s and the focus depth was optimised in order to obtain the highest Raman signal. At least three spectra were acquired for each sample.

2.2.4. NMR spectroscopy

All NMR experiments were performed on a 9.4 T Avance Bruker Spectrometer operating at 79.5 MHz (^{29}Si) and 100.6 MHz (^{13}C). We used a 4 mm diameter rotor spinning at 14 kHz and applied an Hahn–Echo acquisition with a radio-frequency field of 50 kHz (^{29}Si) and 35 kHz (^{13}C) and an inter-pulse delay of 1 rotor period. The relaxation time are found to be around 75 ms for both nuclei because of the presence of iron (1 to 4 wt% on volatile free basis) in the sample. The recycle delays were set to 250 ms, while accumulating between 300 000 and 900 000 scans, depending on the amount of sample available. A Teflon spacer was used to position the sample in the middle of the rotor when using small amounts.

2.3. First principles MD simulations

First-Principles Molecular Dynamics (FPMD) simulations were performed on two systems. The first one is a simplified TA10 system (32 wt% SiO_2; expressed on a volatile-free basis; cf. Table 1) composed of SiO_2 ($x = 0.30$), Al_2O_3 ($x = 0.07$), MgO ($x = 0.14$) CaO ($x = 0.44$) and K_2O ($x = 0.05$) (were x refers to the mole fraction of each component). A simulation box with a side length $L = 14.7$ Å was used. This box consisted of 238 atoms (135 O, 31 Si, 7 Al, 15 Mg, 45 Ca and 5 K). This gave a density of 2.92 g/cm^3. The system was run at $T = 1773$ K. The second system is a simplified TA10 composition containing 13.8 wt% of CO_2, which translates in terms of mole fractions to CO_2 ($x = 0.18$), SiO_2 ($x = 0.25$), Al_2O_3 ($x = 0.05$), MgO ($x = 0.12$), CaO ($x = 0.36$) and K_2O ($x = 0.04$). In this case the simulation box contained 304 atoms (179 O, 31 Si, 7 Al, 15 Mg, 45 Ca, 5 K and 22 C) and its side length measures $L = 15.7$ Å, corresponding to a density of 2.83 g/cm^3. For this system, we fixed the temperature at $T = 1498$ K. The adopted temperature conditions represent melt conditions almost identical to glass syntheses conditions. The experimental glass structure however is that preserved at the glass transition temperature, which is lower than the synthesis temperature, while the structure observed by FPMD is that of the melt. The simulations reported required the use of about 215 000 single CPU hours, using the high performance of the IDRIS supercomputer. Additional simulation details are given in the supplementary information.

Theoretical NMR spectra were obtained from calculations performed on MD boxes, details are given in the supplementary information.

3. Results

Five starting compositions were saturated with CO_2, at pressures from 0.1 to 1500 MPa. This allowed us to create samples of similar compositions with variable CO_2 content. All experiment are reported in Table 2. Analytical data from pressure between 100 to 350 MPa are from the experiments reported in Moussallam et al. (2014). The FPMD ab-initio molecular dynamic simulations were performed on a single composition (with 32 wt% SiO_2 on a volatile free basis) equilibrated at a single pressure, with and without CO_2.

3.1. Infrared spectroscopy

Infrared spectra for CO_2-bearing glasses ranging in composition from 24 to 44 wt% SiO_2 (expressed on a volatile-free basis) are reported in Fig. 1 together with an infrared spectrum obtained on a pure carbonate glass of composition 50:50 mol% $MgCO_3$–K_2CO_3. In all compositions investigated CO_2 in the glass is in the form of carbonate, in contrast to recent findings in water-saturated carbonate melts (Foustoukos and Mysen, 2015). The absence of absorption peak at ~2350 cm^{-1} in all spectra shows the absence of molecular CO_2 in the quenched glass, although it may have been present in the melt (see section 3.4). The carbonate v_3 doublet has a similar position across composition (mid-point at ~1460 cm^{-1}) with a splitting of $\Delta v_3 \approx 70$ cm^{-1}. In detail, small variations between peak position occur from the most silica-rich (TA12; 44 wt% SiO_2 on a volatile free basis) to the most silica-poor glass (TA6; 24 wt% SiO_2 on a dry basis) with the mid-point shifting from 1465 to 1455 cm^{-1} and the Δv_3 split shifting from 80 to 60 cm^{-1}. The spectra obtained on pure carbonate glass shows a mid-point at 1450 cm^{-1} and a splitting of $\Delta v_3 \approx 60$ cm^{-1}.

3.2. Raman spectroscopy

Raman spectra of quenched glasses ranging in composition from 24 to 44 wt% SiO_2 (expressed on a volatile-free basis) and containing 0 to 22 wt% CO_2 are presented in Fig. 2 in the frequency range 700 to 1200 cm^{-1}. All glasses containing CO_2 show a strong peak at ~1080 cm^{-1} corresponding to the stretching of C–O vibration in CO_3^{2-} configuration while no evidence

Table 2
Run conditions, EMPA analyses (averaged from 20), H_2O and CO_2 determined by elemental analyser (Flash) all reported in wt%. Experiments at pressure between 100 to 350 MPa are from Moussallam et al. (2014). Standard deviations are reported in Table S1.

Sample	Pressure (MPa)	Temperature (°C)	SiO_2	TiO_2	Al_2O_3	FeO	MnO	MgO	CaO	Na_2O	K_2O	P_2O_5	Total	Shortfall	H_2O (Flash)	CO_2 (Flash)
TA6_1_1	357.2	1225	18.4	0.2	2.1	0.7	0.0	6.9	45.3	0.3	2.3	0.0	76.2	23.8	1.2	21.8
TA6_1_4	178	1220–1260	18.0	0.2	2.6	0.8	0.0	6.8	44.8	0.4	2.2	0.0	75.8	24.2	0.9	20.1
TA6_2_2	101.7	1225	20.1	0.2	2.8	0.5	0.0	7.0	47.3	0.4	2.0	0.2	80.5	19.5	1.1	17.2
TA9_1_1	336.4	1225	26.1	0.4	5.7	1.5	0.0	8.2	36.9	0.5	3.3	0.1	82.5	17.5	1.2	14.9
TA9_1_2	100.7	1225	24.5	0.5	4.4	1.9	0.0	8.1	39.8	0.5	4.2	0.1	84.2	15.8	0.4	10.1
TA9_1_0	0.1	1500	32.9	0.5	7.8	2.1	0.0	10.0	42.5	0.3	1.9	0.2	98.5	1.5	0.0	0.0
TA10_1_3	1500	1350	26.2	0.4	5.5	0.8	0.0	8.3	33.9	0.3	4.2	0.2	80.0	20.0	0.4	18.3
TA10_1_1	336.4	1225	26.8	0.4	5.8	1.6	0.1	8.5	36.2	0.4	3.4	0.1	83.3	16.8	1.3	13.8
TA10_1_0	0.1	1500	32.6	0.5	7.7	2.2	0.0	10.1	42.2	0.5	2.6	0.2	98.5	1.5	0.0	0.1
TA11_1_3	1500	1350	32.5	0.6	7.4	1.7	0.0	9.5	28.5	0.7	4.3	0.2	85.5	14.5	1.2	12.0
TA11_1_1	347.8	1225	34.5	0.6	7.8	2.9	0.1	10.0	29.1	0.7	4.4	0.1	90.0	10.0	0.8	7.5
TA11_1_2	101	1225	34.7	1.0	9.9	3.9	0.1	8.2	26.5	0.7	6.3	0.2	91.4	8.6	0.4	2.6
TA11_1_0	0.1	1500	37.5	0.7	8.7	2.8	0.1	10.7	32.5	0.5	4.4	0.3	98.3	1.7	0.0	0.0
TA12_1_4	1500	1350	43.0	0.9	9.9	3.3	0.1	9.6	20.7	0.9	5.5	0.5	94.4	5.6	0.4	4.5
TA12_1_1	347.8	1225	41.0	0.8	9.7	3.7	0.1	9.4	23.0	0.8	5.6	0.2	94.2	5.8	0.5	2.8
TA12_1_3	101	1225	43.2	0.9	9.8	3.8	0.1	9.8	22.1	1.0	5.7	0.2	96.6	3.4	0.4	1.0
TA12_1_0	0.1	1500	42.8	0.9	10.2	3.7	0.1	10.3	24.0	0.7	5.3	0.3	98.3	1.7	0.0	0.0

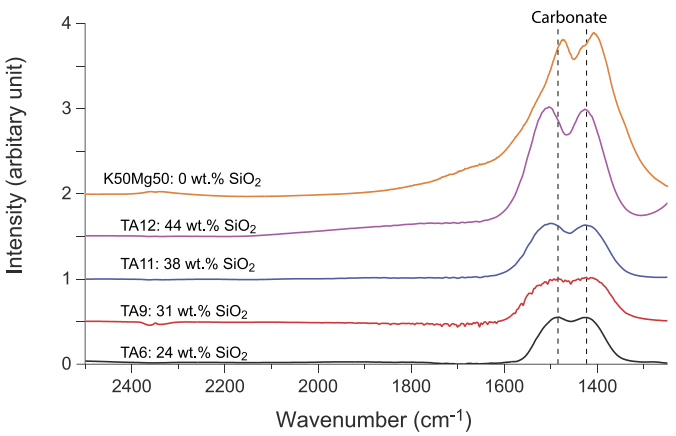

Fig. 1. Infrared spectra for CO_2-bearing glasses ranging in composition from 24 to 44 wt% SiO_2 (expressed on a volatile-free basis). The carbonate ν_3 doublet can clearly be seen in all compositions with a splitting of $\Delta\nu_3 \approx 60$–80 cm^{-1}. The absence of any peak at ~2350 cm^{-1} in all infrared spectra testifies of the absence of molecular CO_2. Dotted lines have been drawn through the TA6 composition (24 wt% SiO_2 on a volatile free basis) carbonate peaks. The infrared spectra of a pure carbonate glass of composition 50:50 mol% $MgCO_3$–K_2CO_3 is also shown for reference. This spectra shows a mid-point at 1450 cm^{-1} and a splitting of $\Delta\nu_3 \approx 60$ cm^{-1}.

for CO_2^{mol} was observed in the Raman spectra at ~1400 cm^{-1} (Mysen and Virgo, 1980a; Sharma, 1979; Verweij et al., 1977; White, 1974) consistent with FTIR spectra shown in Fig. 1. Besides the 1084 cm^{-1} peak, the Raman spectra shown in Fig. 2 can be considered as a complex convolution of individual Gaussian peaks; each corresponding to a given Q^n species (e.g. Mysen, 1990, 2007; Mysen and Cody, 2005; Mysen and Richet, 2005 and references therein). It is clear from Fig. 2 that the addition of CO_2 strongly modifies the shape of the Raman spectra in all investigated compositions. Deconvolution of the high-frequency envelope (800–1200 cm^{-1}) in which 1st-order Raman scattering of (Si, Al)–O stretching vibration occurs is shown in Fig. 3. Deconvolution of Raman spectra is an inherently interpretative process with non-unique solution, all results are hence treated in a purely qualitative sense. Measured Raman spectra are simulated by four individual Gaussian peaks for volatile-free glasses and with a fifth peak at ~1080 cm^{-1} for the ν_1 CO_3^{2-} vibrational signature in CO_2-bearing glasses. Assigning (Si, Al)–O stretching frequency to particular Q-species is not straightforward as the frequency of each band varies as a function of melt chemistry. There is a general consensus however that higher-order (more polymerised) Q-species show (Si, Al)–O stretching at higher frequency than lower-order (less polymerised) Q-species. Here we assign the band near 968 cm^{-1} (marked in orange in Fig. 3) to (Si, Al)–O- stretch vibrations in Q^2-species (in accordance with Brawer and White, 1975; Furukawa et al., 1981; Mysen, 2007; Mysen et al., 1982; Mysen and Cody, 2005), the band near 910 cm^{-1} (marked in green in Fig. 3) to (Si, Al)–O- stretch vibrations in Q^1-species (in accordance with Mysen, 2007) and the band near 860 cm^{-1} (marked in cyan in Fig. 3) to (Si, Al)–O- stretch vibrations in Q^0-species (in accordance with Mysen et al., 1982). The band at ~1025 cm^{-1} is assigned to Si–O^0 vibration in any structural unit with bridging oxygen (in accordance with Mysen et al., 1982). In the fits reported in Fig. 3, band positions were fixed for a given composition while bandwidth, and band intensity were treated as independent variables. Minimum χ^2 was used as the principal convergence criterion. It is clear from Figs. 2 and 3 that for all investigated compositions, the addition of CO_2 results in a change of the glass structure towards more polymerised configurations.

3.3. NMR spectroscopy

^{13}C NMR spectra of compositions ranging from 24 to 44 wt% SiO_2 (expressed on a volatile-free basis), produced at 350 MPa and containing 0 to 22 wt% CO_2 are shown in Fig. 4 together with the ^{13}C NMR spectra of a pure carbonate glass of composition 50:50 mol% $MgCO_3$–K_2CO_3. Peak parameters are given in Table S3 in the supplementary information. All spectra show a single symmetric peak at ~168 ppm indicating that CO_2 is dissolved as carbonate. No evidence of CO_2^{mol} was observed in the ^{13}C spectra at 125 ppm.

^{29}Si NMR spectra of the same glasses are presented in Fig. 5 (Note that the CO_2-free TA9 sample is slightly affected by quench crystal nuclei, slightly distorting the NMR spectra). The solution of ~3 wt% CO_2 to the most silica-rich composition (44 wt% SiO_2 on a volatile-free basis) and from 17 to 22 wt% CO_2 in the most silica-poor composition (24 wt% SiO_2 on a volatile-free basis) results in no discernible change to the ^{29}Si chemical shift in glasses. For compositions with 38, 32 and 31 wt% SiO_2 (expressed on a volatile-free basis), the solution of 7.5, 13.8 and 14.9 wt% CO_2 (corresponding to 10, 18 and 19 mol% CO_2 respectively) results in a significant shift of the peak maximum of the ^{29}Si spectra of 3 to

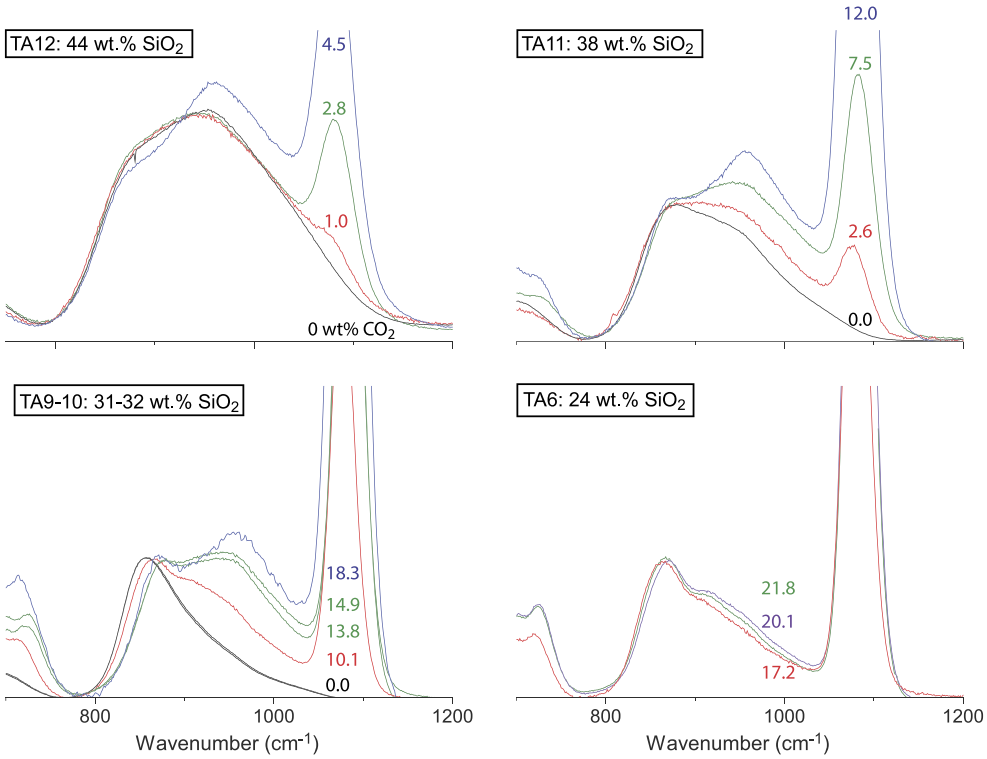

Fig. 2. Raman spectra of quenched glasses ranging in composition from 24 to 44 wt% SiO_2 (expressed on a volatile-free basis) and containing 0 to 22 wt% CO_2 in the frequency range 700 to 1200 cm^{-1}. Spectra are coloured based on the pressure at which each glass was synthesised with black, red, violet, green and blue corresponding to experiments performed at 0.1, 100, 175, 350 and 1500 MPa respectively. The CO_2 content of each glass is reported next to its spectra in corresponding colour. All glasses containing CO_2 show a strong peak at 1084 cm^{-1} corresponding to the stretching of C–O vibration in CO_3^{2-} configuration. No evidence for CO_2^{mol} was observed in any Raman spectra at ~1400 cm^{-1} (Brooker et al., 1999). (For interpretation of the references to color in this figure legend, the reader is referred to the web version of this article.)

5 ppm towards more negative values and an even more drastic shift of the centre of mass of 4 to 7 ppm towards more negative values. The asymmetry of these peaks also changes becoming skewed towards more negative values of ^{29}Si chemical shift with increasing CO_2 content. The ^{29}Si spectra shown in Fig. 5 can be considered a complex convolution of individual peaks; each corresponding to a given $Q^n(p\text{Al})$ species (where n denotes as usually the number of bridging oxygen on the Q unit and p the number of connected aluminium atoms (hence a Q^n species with p Si–O–Al bridges and $(n-p)$ Si–O–Si ones) (e.g. Hiet et al., 2009; Lee and Stebbins, 1999; Lippmaa et al., 1981, 1980; Maekawa et al., 1991; Magi et al., 1984; Engelhardt and Michel, 1987; Morizet et al., 2015, 2014a). The resonance frequency of $Q^n(p\text{Al})$-species however varies as a function both n and p but in opposite direction resulting in ambiguities in the band assignment in ^{29}Si NMR spectra across composition. For this reason we restrain from using NMR spectra to quantify the observed chemical shift in terms of changes in Q^n-species.

3.4. First principle MD simulations

Two first principles molecular dynamic (FPMD) simulations were performed on a single composition (32 wt% SiO_2; expressed on a volatile-free basis). Simulations were performed on the base composition with 13.8 wt% and 0 wt% CO_2 respectively. Fig. 6 shows a snapshot of the last configuration extracted from both FPMD simulations (Figs. 6A and 6B). FPMD simulation on the CO_2-bearing composition shows that CO_2 is dissolved dominantly as carbonate species with very few CO_2^{mol} (Fig. 6F). The silicate structure from both simulations is shown in Fig. 6C and Fig. 6D. The silicate network from both simulations appears clearly distinct with the CO_2-bearing simulation being more polymerised than the CO_2-free simulation. The average number of NBO/Si decreases from 3.4 in the CO_2-free simulation to 2.8 in the simulation with 13.8 wt% CO_2. When considering also NBO-carb the number of NBO decreases further to 2.7 (Fig. 6E).

Simulations of the ^{29}Si NMR spectra were produced using results from FPMD simulations (see supplementary information). Fig. 7 compares the simulated spectra with the spectra obtained on the corresponding experimentally quenched glasses. The agreement between the simulated FPMD-based NMR spectra and the spectra obtained on the corresponding experimental glasses is excellent (considering the limited number of atoms – and hence statistics – on which the NMR calculations could be performed), confirming that the molecular structure resulting from FPMD simulations reproduces the structure of the silicate network of the experimental system and that the experimental glasses preserved the structure present in the melt conditions. The agreement between FPMD-simulated and measured NMR spectra is best for the composition with 13.8 wt% CO_2 as four FPMD simulations were used to calculate the NMR spectra compared to two FPMD simulations used for the composition with 0 wt% CO_2. The same procedure has been applied to the ^{13}C spectra, and as can also be seen from Fig. 7 the result is satisfactory. The asymmetry displayed by the calculated spectra indicates the small but significant abundance of CO_3 groups linked to the aluminosilicate network with a bridging oxygen (NBO-carb.; Brooker et al., 2001b) in the FPMD simulation and which are not apparent (or not preserved during quenching) in the experimental glass.

4. Discussion

4.1. Carbon dioxide speciation and environment in transitional melts

4.1.1. Carbon dioxide speciation

Infrared spectra show that carbon dioxide in the investigated compositions is present in the glass (quenched from melt) as

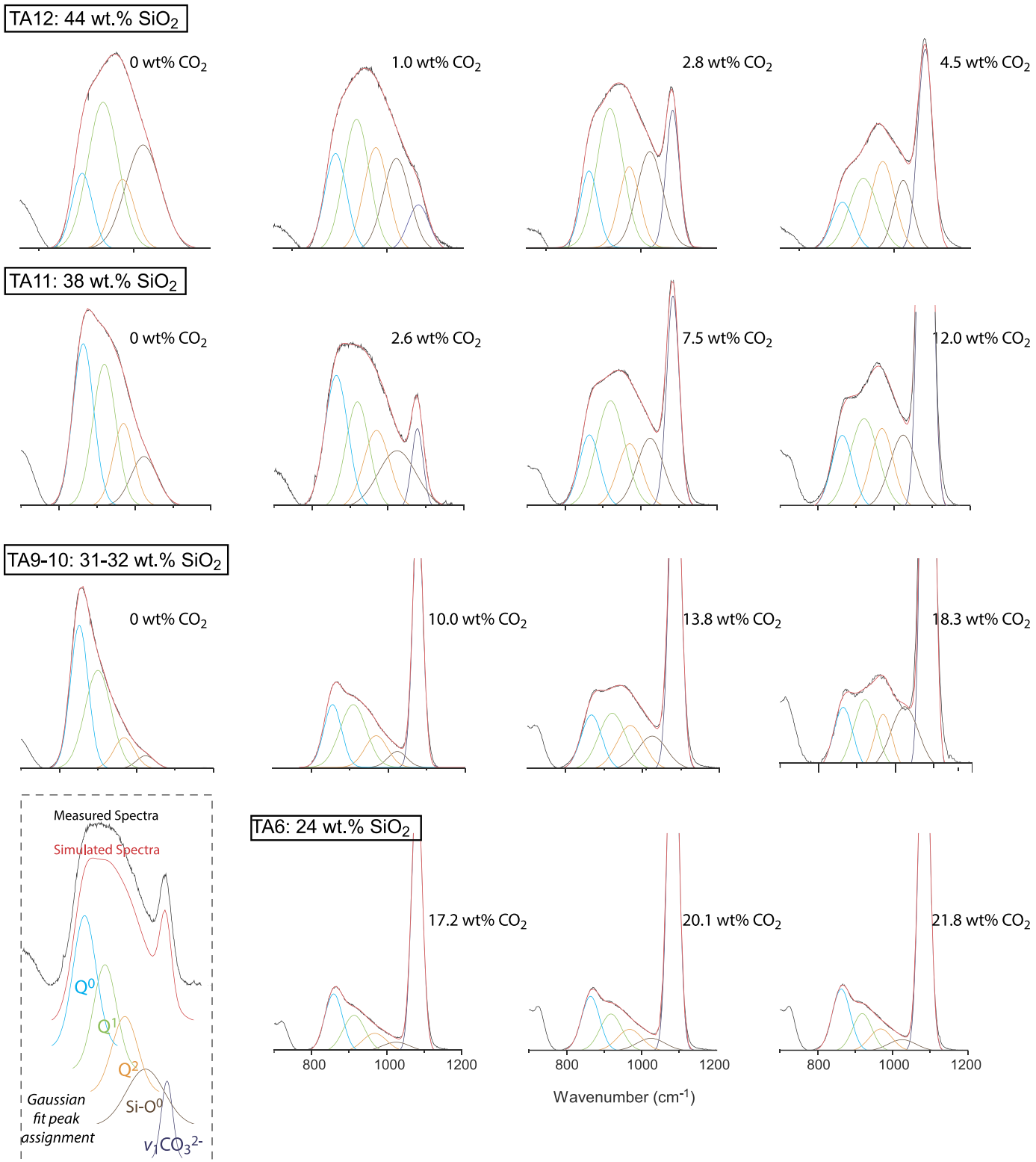

Fig. 3. Raman spectra obtained on quenched glasses ranging in composition from 24 to 44 wt% SiO_2 (expressed on a volatile-free basis) and containing 0 to 22 wt% CO_2. The high-frequency envelope (800–1200 cm^{-1}) is simulated by four individual Gaussian peaks for volatile-free glasses and with a fifth peak at ~1080 cm^{-1} for the ν_1 CO_3^{2-} vibrational signature. Spectra convolution and peak assignment is illustrated in the lower left inset. Peak assignment follows Mysen (1990, 2007) and Mysen and Cody (2005) (see references therein) and is discussed in the text. (For interpretation of the colors in this figure, the reader is referred to the web version of this article.)

carbonate. Raman spectra confirm that carbon dioxide is only present as CO_3^{2-} in all investigated glasses. ^{13}C NMR spectra also show that CO_2 is dissolved in all investigated glasses as carbonate group. We found no evidence for the presence of CO_2^{mol} at 125 ppm.

In mafic silicate glass, carbon dioxide typically dissolves as carbonate ion (CO_3^{2-}) (e.g. Fine and Stolper, 1986). An increasing amount of evidence however suggest that carbon dioxide may actually not entirely dissolve as CO_3^{2-} in the more common silicate melt compositions, including basalts. Annealing ex-

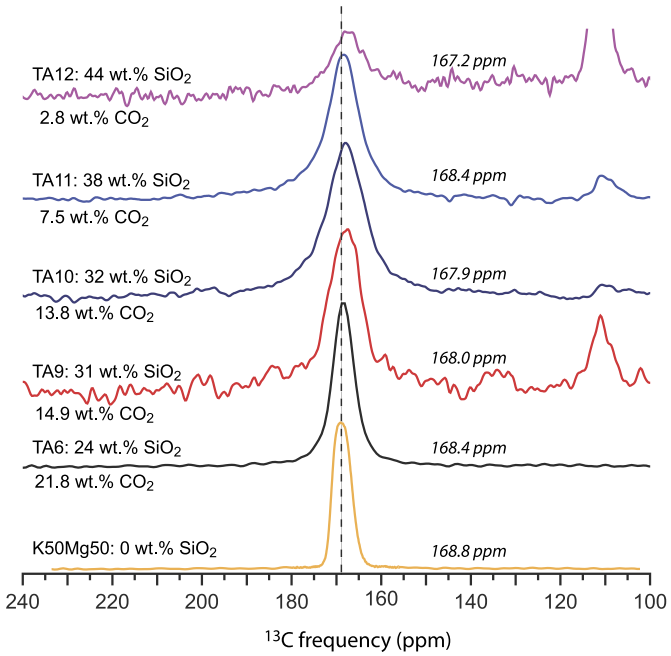

Fig. 4. ^{13}C NMR spectra obtained on quenched glasses ranging in composition from 24 to 44 wt% SiO_2 (expressed on a volatile-free basis) and containing 0 to 22 wt% CO_2. The NMR spectra of a pure carbonate glass of composition 50:50 mol% $MgCO_3$–K_2CO_3 is also shown for reference. All spectra can be described as a single Gaussian peak, the centre of which is reported (in ppm) beside each spectra. At the resolution considered there is no difference in the ^{13}C chemical shift across investigated compositions. The peak at 110 ppm apparent in some spectra is an artefact resulting from the use of Teflon as a sample holder. Peak parameters are given in Table S3.

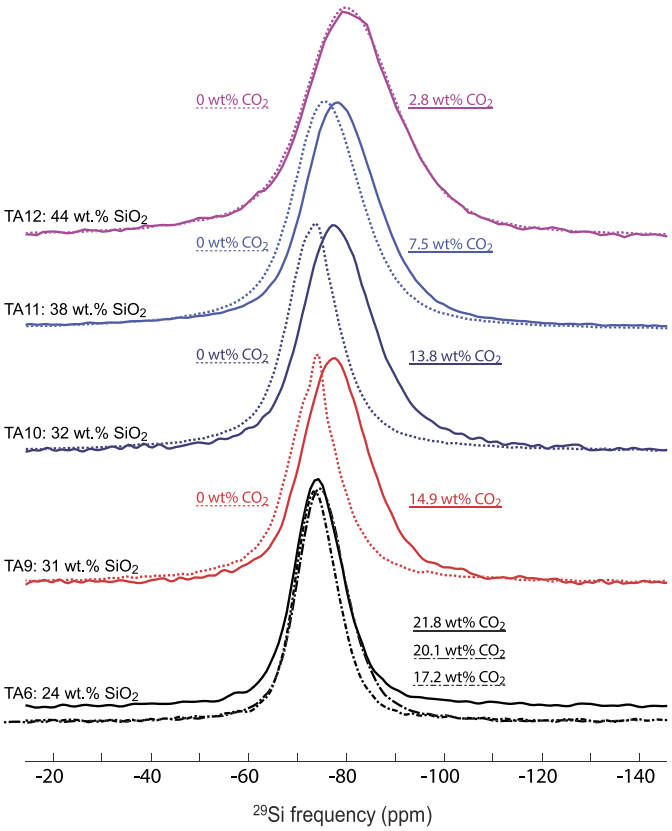

Fig. 5. ^{29}Si NMR spectra obtained on quenched glasses ranging in composition from 24 to 44 wt% SiO_2 (expressed on a volatile-free basis) and containing 0 to 22 wt% CO_2. The CO_2 content of each glass is reported next to its spectra in corresponding colour. Dotted lines are from CO_2-free glasses. Peak parameters are given in Table S3.

periments – performed below the glass transition temperature (T_g) – on CO_2-bearing jadeite (Morizet et al., 2001), albitic and dacitic (Nowak et al., 2003) glasses show that the equilibrium between molecular and carbonate species shifts towards molecular CO_2 with increasing temperature. Molecular dynamics simulations by Guillot and Sator (2011) and Morizet et al. (2015) confirmed that the mole fraction of molecular CO_2 in basaltic melt increases with temperature, while carbonate ions are the only species observed in basaltic glasses, a significant amount of molecular CO_2 is present in the melt. A recent in-situ infrared spectroscopy study by Konschak and Keppler (2014) studied the speciation of carbon dioxide in diamond anvil cell experiments up to 1000 °C, confirming that the $CO_2 + O^{2-} = CO_3^{2-}$ equilibrium in the melt shift towards CO_2 with increasing temperature in dacite and phonolite melts (at this time no similar experiments on basaltic composition have been performed).

Given the silica-poor composition investigated here, the speciation of carbon dioxide as CO_3^{2-} in the glass is fully consistent with previous studies (e.g. Brooker et al., 2001b; Ni and Keppler, 2013). The speciation of carbon dioxide in the melt could be different to that preserved in the glass (which preserves the structure at the glass transition temperature) and was investigated by FPMD simulations, showing that ~90% of carbon in the investigated composition is stable as carbonate (Fig. 6F). This is consistent with previous studies suggesting that for the low-silica composition investigated most of the CO_2 should also be dissolved as CO_3^{2-} in the melt (e.g. Konschak and Keppler, 2014; Ni and Keppler, 2013; Vuilleumier et al., 2015).

4.1.2. Carbon dioxide environment

The mid-point of the carbonate ν_3 doublet at 1460 cm^{-1} and split of $\Delta\nu_3 = 60$–80 cm^{-1} in the infrared spectra is close to that found in most Ca-bearing silicate melts (Brooker et al., 2001b). Blank and Brooker (1994) and Brooker et al. (2001b) have suggested that NBO-carbonate species (in which a carbonate group is linked to a Si tetrahedra via a non-bridging oxygen) can produce ν_3 splitting of the order $\Delta\nu_3 = 70$–100 cm^{-1}. We show however that $\Delta\nu_3$ split of 60 cm^{-1} can be observed in pure carbonate glass were carbonate group are not linked to any silica tetrahedra, and consistently with Sharma and Simons (1980) and White (1974). This illustrates, that the ν_3 splitting is only function of the degree of distortion of the carbonate group, its absolute value therefore does not necessarily imply chemical bonding to a specific ion. Another possible interpretation is that the observed ν_3 'doublet' might represent two distinct symmetrical site with different surrounding cations (in this case Mg or K) rather than the lifting of ν_3 degeneracy by distortion. Indeed Genge et al. (1995) suggested than in pure carbonate melts, CO_3^{2-} groups interact strongly with Ca and Mg cations and less strongly with alkalies. ^{13}C NMR spectra show that in all investigated compositions a single symmetric peak centred at ~168 ppm is present, suggesting a single environment for CO_3^{2-} or that NMR is insensitive to any difference. This peak position was found in CO_2-bearing nepheline, albite and sodamelilite melt by Kohn et al. (1991), in nepheline, jadeite and albite melt by Brooker et al. (1999), in haplo-phonolites by Morizet et al. (2002) in amorphous calcium carbonate by Nebel et al. (2008) in nephelinite by Morizet et al. (2014a, 2014b) and diopside and Ca-melilitite by Morizet et al. (2015) who attributed it to NBO-carbonate species (where a CO_3^{2-} molecule is connected to a NBO and charge compensated by a surrounding cation). The presence of the same peak position in pure carbonate glass (Fig. 4), close to that of common carbonate minerals (e.g. Papenguth et al., 1989), however argues against such definite designation. The ^{13}C chemical shift we identify in transitional glasses is indistinguishable from that found in

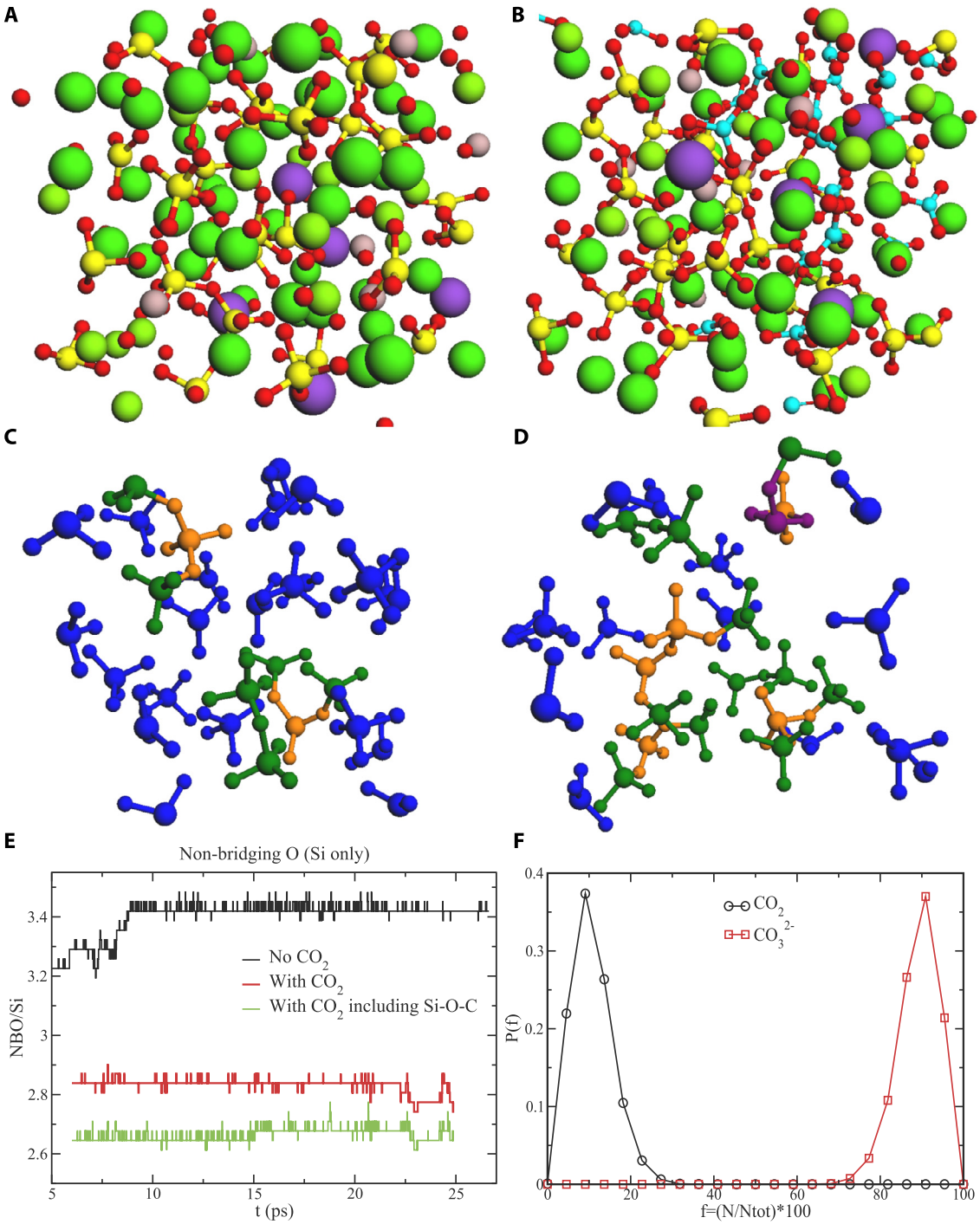

Fig. 6. Snapshot of the last configuration extracted from first principles molecular dynamic (FPMD) simulations on a TA10 composition (32 wt% SiO_2; expressed on a volatile-free basis) equilibrated with 0 wt% CO_2 (**A**) and 13.8 wt% CO_2 (**B**). Carbon atoms are in blue, oxygen atoms are in red, silicon atoms are in yellow, aluminum atom are in light brown, Ca atoms are in green (large balls), Mg atoms are in light green (smaller balls), K atoms are in purple. The atomic radii drawn are proportional to the van der Waals radii. Snapshot of the silicate network solely is shown for both simulations with 0 wt% CO_2 (**C**) and 13.8 wt% CO_2 (**D**) with silica tetrahedra coloured based on the number of shared oxygen as follow: blue for no shared oxygen (i.e. Q^0-species), green for one oxygen shared (i.e. Q^1-species), orange for two oxygen shared (i.e. Q^2-species), and purple for three oxygen shared (i.e. Q^3-species). **E**: Plot of the number of non-bridging oxygen divided by the number of Si as a function of simulation time for simulations performed with 0 and 13.8 wt% CO_2. **F**: Probability (calculated over the 20 ps of simulation time) of having a fraction of C atoms involved in CO_2^{mol} (black) or CO_3^{2-} (red). (For interpretation of the references to color in this figure legend, the reader is referred to the web version of this article.)

a pure carbonate glass suggesting that CO_3^{2-} groups are located in a similar environment (i.e. as free carbonate). Moreover, the barycentre of the ^{13}C NMR component of NBO-carbonate species found in the MD simulation resonate at −1.4 ppm for CO_3–Al and −4.3 ppm for CO_3–Si with respect to that of isolated CO_3 units (see Fig. 7). In other words if the presence of iron broadens the NMR line to the point where we cannot expect to resolve those species, those shifts are big enough that a significant amount of NBO-CO_3 units should produce an asymmetry in the ^{13}C NMR line on its right tail, in contradiction with the fully symmetric observed line. Bridging carbonate species (Si–carb–Si), also referred to as "network carbonate" are particularly unlikely to be present in the observed glass as such highly distorted species would have been clearly identifiable in the infrared (characterised by large Δv_3 split

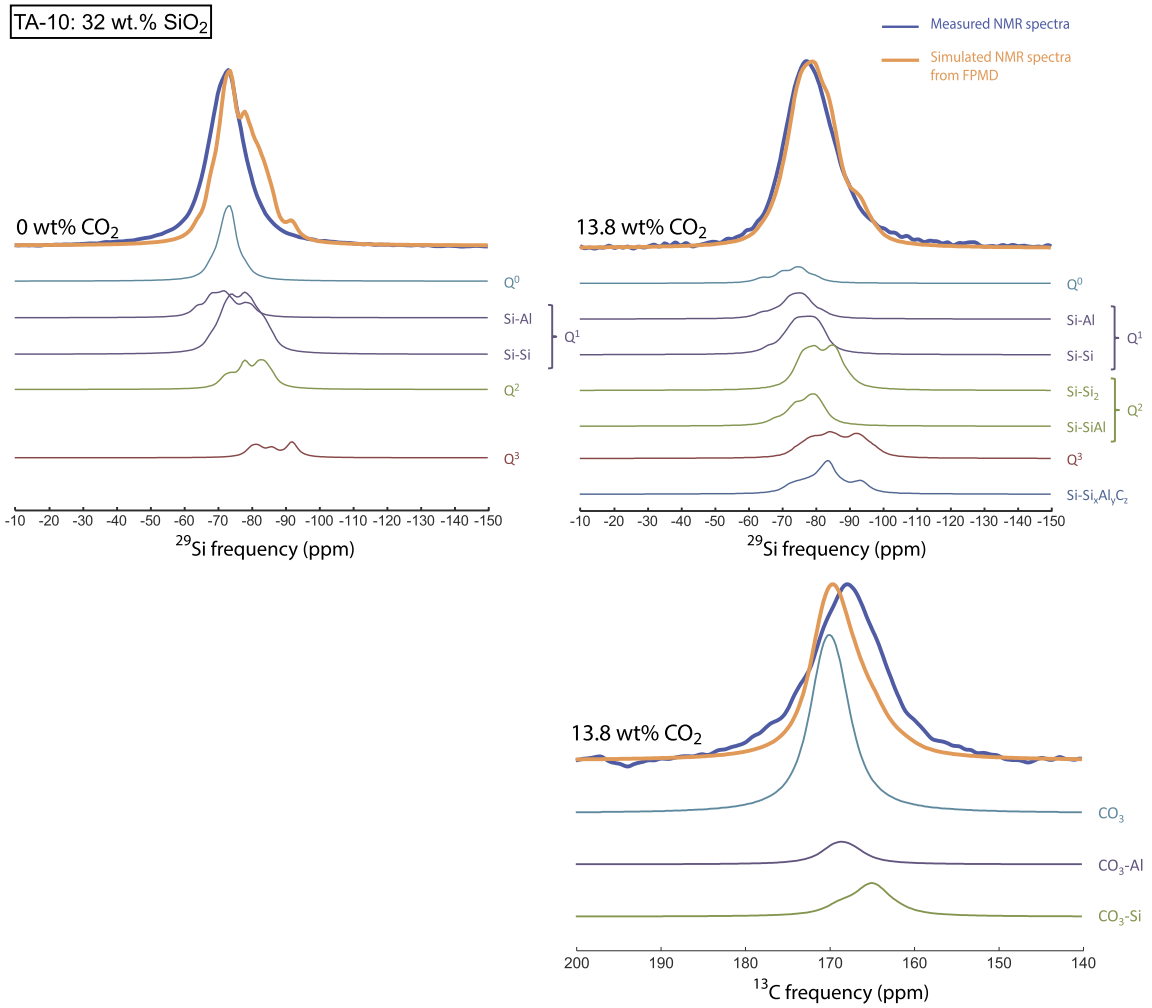

Fig. 7. Upper two panels: ^{29}Si NMR spectra obtained on quenched glasses with 32 wt% SiO_2 (expressed on a volatile-free basis) and containing 0 and 13.8 wt% CO_2 compared to simulated ^{29}Si NMR spectra obtained from FPMD simulations on the same composition. The deconvolution of the simulated ^{29}Si NMR spectra is shown in term of simulated contribution from $Q^n(p\text{Al})$-species. Note that simulated ^{29}Si NMR spectra are based on four and two FPMD simulations for the compositions with 13.8 and 0 wt% CO_2 respectively explaining the lesser spectrum quality for the composition with 0 wt% CO_2. Lower panel: ^{13}C NMR spectra obtained on quenched glasses with 32 wt% SiO_2 (expressed on a volatile-free basis) and 13.8 wt% CO_2 compared to simulated ^{13}C NMR spectra obtained from FPMD simulations. Note that the discrepancy between the two spectra lies in the asymmetry displayed by the calculated spectra which is due to the non-negligible presence of CO_3 groups linked to the aluminosilicate network (NBO-carb) in the FPMD simulation. NBO-carb groups are not apparent (or not preserved during quenching) in the experimental glass. The signal of the experimental glass spectrum is broader than the simulated spectrum due to the presence of Fe.

~150–300 cm^{-1}; Brooker et al., 1999, 2001b) and ^{13}C NMR spectra (characterised by chemical shift near 155-165 ppm; Morizet et al., 2002, 2014a, 2015; Brooker et al., 1999).

FPMD simulations of the melt predict that most dissolved carbon atoms form free CO_3^{2-} groups linked to alkaline earth cations (i.e. are in the same environment than in a pure carbonate; not linked to the silicate network). Few NBO-carbonate are predicted to be stable and no network carbonate species was found to be stable. These findings are consistent with previous molecular dynamic simulation performed by Vuilleumier et al. (2015) on kimberlite melt and with our infrared and ^{13}C NMR spectroscopic results and suggest that the environment of CO_3^{2-} in transitional glasses and melts is dominantly as free carbonates. Those results are also consistent with the current knowledge suggesting that network carbonate are stable in more polymerised (more silica rich) compositions.

4.2. *Effect of carbon dioxide on transitional melts polymerisation*

It is clear from both Raman and NMR investigations that the addition of CO_2 has a drastic effect on the glass structure, systematically modifying it to more polymerised configuration by sequestering metal cations from their usual depolymerising role (Figs. 3 and 5). FPMD simulations and the resulting calculation of NMR parameters also are consistent with CO_2 dissolution modifications of the network structure to a more polymerised configuration (Figs. 6 and 7). This effect appears to be minimal to insignificant for the addition of up to ~3 wt% CO_2 in the most silica-rich composition investigated and for changes from 17.2 to 21.8 wt% CO_2 in the most silica-poor composition investigated. Using the relative area defined by each band used in the Raman spectra deconvolution, the relative abundance of each Q-species as a function of CO_2 content can be expressed. We stress that such estimate of Q-species proportion from Raman spectra can only be qualitative.

We also stress that the change seen in both Raman and ^{29}Si NMR spectra could be interpreted in different ways from the increase in glass polymerisation corresponding to topological changes (Massiot et al., 2013). For instance, both Raman and ^{29}Si NMR spectra could be affected by the electrical charge distribution due to the nearby presence of CO_3^{2-} group therefore distorting the geometry of the Q^n cluster (Massiot et al., 2013). Those geometrical changes (change in bond lengths and bond angles) have been recognised to affect in a significant way the

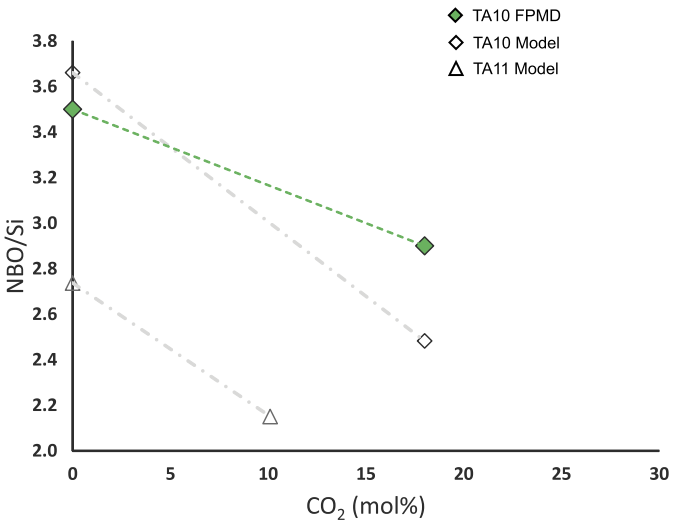

Fig. 8. Evolution of the degree of polymerisation of the glass (expressed as NBO/Si) as a function of dissolved mol% CO_2 as calculated from FPMD simulations. Open symbols and dash-dot grey lines correspond to theoretically calculated NBO/Si assuming that the addition of CO_2 removes an oxygen from the silicate network hence increasing its polymerisation.

^{29}Si NMR chemical shift. For instance, the presence of Al atom around a Si Q^n species can induce a shift of +5 ppm in the ^{29}Si chemical shift as compared to a similar Q^n species without Al atom in the first coordination shell (Hiet et al., 2009; Schmidt et al., 2000). Cations serving as charge-balancers for tetrahedrally-coordinated Al^{3+} might interact with CO_3^{2-} to form isolated carbonate complexes hence changing the structural role of Al^{3+} thus changing the shielding of the silicon-29 nucleus. We see such alternative while certainly plausible, as less likely and as a more tortuous way of interpreting the spectra. At present, too little data on such effect are available for such hypothesis to be rigorously tested.

The decrease in the ^{29}Si NMR line position (i.e. barycentre) is either due to a change in the $Q^n(p\text{Al})$ populations or eventually to a shift of those components due to the addition of CO_2. Although not much is experimentally known about the effect of the proximity of CO_3 units on the ^{29}Si NMR line position, one can get an idea using the species found by MD simulations. Considering only the evolution of their centre of mass, adding CO_2 leads to a ^{29}Si line shift of −0.2 ppm, 0.5 ppm, −2.3 ppm, −1.7 ppm and 0.2 ppm for $Q^0(0)$, $Q^1(0)$, $Q^1(1)$, $Q^2(0,1,2)$ and $Q^3(0,1,2)$ species respectively (i.e. the maximum line position is 170.0 ppm for isolated $^{13}CO_3$, 168.6 ppm for $^{13}CO_3$–NBO(Al) and 165.0 ppm for $^{13}CO_3$–NBO(Si) (see Fig. 7, bottom right spectra). In other words it is unlikely that a "chemical" effect of the CO_3 groups on the individual $Q^n(p)$ units can explain the observed −4 to −7 ppm shift in the ^{29}Si line's centre of mass. Likewise a decrease in p could potentially lead to such evolution, but this means a form of phase separation where the aluminium atoms are segregated from the silica network, a chemical hypothesis we have no reasons to consider here. The most likely explanation is hence an increase in the population of the highly polymerised species. It is also interesting to note that according to those simulations substituting a C atom to an Si atom on a $Q^2(0,1)$ units leads to a shift of approximately −3 ppm (we do not have enough of those species in the MD boxes to extract a precise value), i.e. silicon linked to CO_3 groups cannot be resolved on the ^{29}Si NMR spectra of the glasses.

The small amount of water (always <1.2 wt% H_2O) present in the final run product cannot explain the extant of the observed signal. Whilst experiments were conducted at a range of pressure (0.1 to 1500 MPa), it is unlikely that such variation could explain the measured signal. We note finally that the null-hypothesis; that dissolution of CO_2 does not affect the degree of polymerisation of the melt and resulting glass would predict that both Raman and NMR spectra should result in line shapes more consistent with an increasingly depolymerised structure with the addition of CO_2 (due to dilution of the aluminosilicate component with increasing amount of CO_2). The fact that we observe the exact opposite (Raman and NMR spectra shifting to line shape more consistent with an increasingly polymerised structure with the solution of CO_2) argues for a polymerising role of CO_2 on the molecular structure of the compositions investigated. Fig. 8 shows the evolution of the apparent degree of polymerisation of the glass (expressed as NBO/Si) as a function of mol% CO_2 as calculated from FPMD simulation. The extent of the polymerisation of glasses increases with increasing amount of CO_2 (the amount of non-bridging oxygen per silica decreases). The relative change with increasing CO_2 content is apparent in the Raman spectra (Fig. 3), NMR spectra (Fig. 5) and FPMD results (Fig. 6 and Fig. 8). The relationship between NBO/Si and CO_2 content calculated from FPMD simulation (see also Fig. 6E) is of ∼−0.2 for every 5 mol% CO_2 added. If we consider that CO_2 in the melt forms free CO_3^{2-} groups by taking a non-bridging oxygen from the silicate network we can calculate the expected effect on the melt NBO/Si. This theoretical effect is shown for two of the investigated composition in Fig. 8 alongside measurements from FPMD simulations. The predicted effect of CO_2 on the melt NBO/Si matches fairly well that measured by FPMD simulations.

As discussed in section 4.1, our spectroscopic investigations and FPMD simulations suggest that most of the carbon dioxide in transitional melts is dissolved as carbonate ions, in form of free carbonates. This prediction is fully consistent with the polymerisation effect of CO_2 we measure in experimental transitional glasses and observe in FPMD simulations.

4.3. Implications for melt physical properties and mobility

The degree of polymerisation of a melt often can be linked to its physical properties. The density, viscosity and compressibility of silicate melts depend on their degree of polymerisation (Gaskell, 1982; Mysen et al., 1982; Mysen and Richet, 2005). Other properties such as element diffusivity (e.g. Eyring, 1935; Tinker et al., 2004) electrical conductivity (e.g. Pommier et al., 2013) and sound velocity (Sakamaki et al., 2014) can also be related to melt polymerisation.

Our results show that carbon dioxide dissolved in transitional melts increases their degree of polymerisation implying that the physical properties of these melts will be highly dependent on their CO_2 content. The viscosity and density of transitional melt are then expected to be impacted by high CO_2 contents. Whether carbonated melt will ascend, sink or pound in the upper mantle, is dictated by their transport properties and hence, we argue, by their CO_2 content. Geophysical investigations of the upper mantle have defined a laterally continuous layer, the low velocity zone (LVZ), marked by a sharp reduction in seismic wave velocity and elevated electrical conductivity. Both features are sometimes related to melt ponding at the boundary between the rigid lithosphere and ductile asthenosphere (Sakamaki et al., 2013; Schmerr, 2012; Sifre et al., 2014). If the LVZ is indeed a region where melt ponds, there must be a physical reason explaining why such melt would accumulate and not ascend through the lithosphere. A conceivable hypothesis is that carbonated melts, with their higher than expected degree of polymerisation might be more viscous than expected, potentially impeding their rise and making them stall at the LVZ.

Conversely, the removal of CO_2 from a transitional melt will also strongly influence its structure. Ascending transitional melts

such as those generating kimberlites will see their molecular structure change tremendously as a result of CO_2 degassing. Considering these melts could contain several tens of wt% CO_2 originally, they will become increasingly depolymerised as CO_2 is exsolved from the melt. The viscosity of these melts is therefore expected to decrease which should increase their mobility, potentially speeding up their ascent.

The molecular picture of transitional melt we have depicted here, is one in which the addition of CO_2 leads to the formation of free carbonate and an ever more polymerised aluminosilicate network. In essence, this view is one in which two sub-networks, a carbonated and a silicate one are cohabiting but getting increasingly disconnected from each other. This view is consistent with the realisation that many experiments in transitional melt composition result in immiscibility between a silicate and a carbonate liquid (Brooker et al., 2011; Brooker and Kjarsgaard, 2011). Liquid immiscibility might take place once a critical proportion of isolated carbonate groups has been reached.

CO_2 solubility in silicate melts is clearly related to the amount of non-bridging oxygen (e.g. Holloway et al., 1976; Brooker et al., 2001a; Ni and Keppler, 2013), yet the aforementioned effect on CO_2 in transitional melts is to decrease the number of NBO. As transitional melts incorporate CO_2, their structure changes (number of NBO decreases) hence their capacity to dissolve CO_2 decreases. This structural approach can help explaining the very peculiar solubility law of CO_2 in transitional melts highlighted by Moussallam et al. (2014) who found a strongly non-linear dependence of CO_2 solubility to pressure. With increasing pressure CO_2 solubility first increases rapidly but after a certain amount of CO_2 is dissolved, the rate of CO_2 dissolution with increasing pressure diminishes and the pressure-solubility relationship becomes linear and comparable to that of a silicate melt (at least in the pressure range investigated).

5. Summary

We have investigated the structure of transitional (carbon-rich; silica-poor) melts quenched to glass by means of infrared, Raman, ^{13}C and ^{29}Si NMR spectroscopy and first principles molecular dynamic simulations. We have found that carbon in transitional glasses is present as CO_3^{2-}, most likely as free carbonate groups and that the addition of CO_2 strongly modifies the structure of transitional glasses resulting in a strong polymerisation of the aluminosilicate network. The key conclusions we draw from our findings are:

i. In transitional melts the addition of CO_2 results in the formation of free carbonate groups, effectively removing NBOs from the aluminosilicate network, hence forcing polymerisation.
ii. The resulting expected effect on transitional melt properties is an increase of their viscosity with increasing CO_2 content although this effect might be balanced by shear dilution of the aluminosilicate component. Ascent of carbonated melts in the mantle might be impeded by higher than expected melt viscosities and lead to melt ponding at certain levels within the mantle such as at the lithosphere–asthenosphere boundary.
iii. Carbon-rich transitional melts are effectively composed of two sub-networks; a carbonate and a silicate one. This peculiar molecular structure might lead to physical properties of the melt being determined by either sub-network. Electrical conductivity will be high as determined by the purely ionic structure of the carbonate sub-network while diffusivity of network-forming species will be low as determined by the polymerised structure of the silicate sub-network.

Acknowledgements

We thank Rémi Champallier, for assistance in the laboratory. Special thanks also go to Ida Di Carlo for help with the electron probe analyses. Funding for this work was provided by the European Research Council (ERC grant number 279790) and the Agence Nationale de la Recherche (ANR-10-BLAN-62101). We also acknowledge the HPC resources from GENCI–[TGCC/CINES/IDRIS] (Grants 2013-082309, 2014-082309 and 2015-082309). Valuable reviews by Bjørn Mysen, Richard Brooker and an anonymous reviewer improved the quality of the manuscript.

Appendix A. Supplementary material

Supplementary material related to this article can be found online at http://dx.doi.org/10.1016/j.epsl.2015.11.025.

References

Blank, J.G., Brooker, R.A., 1994. Experimental studies of carbon dioxide in silicate melts; solubility, speciation, and stable carbon isotope behavior. Rev. Mineral. Geochem. 30, 157–186.

Brawer, S.A., White, W.B., 1975. Raman spectroscopic investigation of the structure of silicate glasses. I. The binary alkali silicates. J. Chem. Phys. 63, 2421.

Brey, G., Green, D., 1976. Solubility of CO_2 in olivine melilitite at high-pressures and role of CO_2 in earth's upper mantle. Contrib. Mineral. Petrol. 55, 217–230. http://dx.doi.org/10.1007/BF00372228.

Brooker, R.A., Kjarsgaard, B.A., 2011. Silicate–carbonate liquid immiscibility and phase relations in the system SiO_2–Na_2O–Al_2O_3–CaO–CO_2 at 0·1–2·5 GPa with applications to carbonatite genesis. J. Petrol. 52, 1281–1305. http://dx.doi.org/10.1093/petrology/egq081.

Brooker, R.A., Kohn, S.C., Holloway, J.R., McMillan, P.F., Carroll, M.R., 1999. Solubility, speciation and dissolution mechanisms for CO_2 in melts on the $NaAlO_2$–SiO_2 join. Geochim. Cosmochim. Acta 63, 3549–3565. http://dx.doi.org/10.1016/S0016-7037(99)00196-9.

Brooker, R., Kohn, S., Holloway, J., McMillan, P., 2001a. Structural controls on the solubility of CO_2 in silicate melts: part I: bulk solubility data. Chem. Geol. 174, 225–239. http://dx.doi.org/10.1016/S0009-2541(00)00353-3.

Brooker, R.A., Kohn, S.C., Holloway, J.R., McMillan, P.F., 2001b. Structural controls on the solubility of CO_2 in silicate melts: part II: IR characteristics of carbonate groups in silicate glasses. In: 6th International Silicate Melt Workshop. Chem. Geol. 174, 241–254. http://dx.doi.org/10.1016/S0009-2541(00)00318-1.

Brooker, R.A., Sparks, R.S.J., Kavanagh, J.L., Field, M., 2011. The volatile content of hypabyssal kimberlite magmas: some constraints from experiments on natural rock compositions. Bull. Volcanol. 73, 959–981. http://dx.doi.org/10.1007/s00445-011-0523-7.

Dalton, J.A., Presnall, D.C., 1998. The continuum of primary carbonatitic–kimberlitic melt compositions in equilibrium with lherzolite: data from the system CaO–MgO–Al_2O_3–SiO_2–CO_2 at 6 GPa. J. Petrol. 39, 1953–1964. http://dx.doi.org/10.1093/petroj/39.11-12.1953.

Dasgupta, R., Hirschmann, M.M., 2006. Melting in the Earth's deep upper mantle caused by carbon dioxide. Nature 440, 659–662. http://dx.doi.org/10.1038/nature04612.

Dasgupta, R., Mallik, A., Tsuno, K., Withers, A.C., Hirth, G., Hirschmann, M.M., 2013. Carbon-dioxide-rich silicate melt in the Earth's upper mantle. Nature 493, 211–215. http://dx.doi.org/10.1038/nature11731.

Eggler, D.H., 1978. The effect of CO_2 upon partial melting of peridotite in the system Na_2O–CaO–Al_2O_3–MgO–SiO_2–CO_2 to 35 kb, with an analysis of melting in a peridotite-H_2O–CO_2 system. Am. J. Sci. 278, 305–343. http://dx.doi.org/10.2475/ajs.278.3.305.

Engelhardt, G., Michel, D., 1987. High-Resolution Solid-State NMR of Silicates and Zeolites. John Wiley & Sons. 485 pages.

Eyring, H., 1935. The activated complex in chemical reactions. J. Chem. Phys. 3, 107–115. http://dx.doi.org/10.1063/1.1749604.

Fine, G., Stolper, E., 1986. Dissolved carbon dioxide in basaltic glasses: concentrations and speciation. Earth Planet. Sci. Lett. 76, 263–278. http://dx.doi.org/10.1016/0012-821X(86)90078-6.

Foustoukos, D.I., Mysen, B.O., 2015. The structure of water–saturated carbonate melts. Am. Mineral. 100, 35–46. http://dx.doi.org/10.2138/am-2015-4856.

Frost, D.B.R., Frost, D.C.D., 2013. Essentials of Igneous and Metamorphic Petrology, 1 edition. Cambridge University Press, New York.

Furukawa, T., Fox, K.E., White, W.B., 1981. Raman spectroscopic investigation of the structure of silicate glasses. III. Raman intensities and structural units in sodium silicate glasses. J. Chem. Phys. 75, 3226.

Gaskell, D.R., 1982. The densities and structures of silicate melts. In: Saxena, S.K. (Ed.), Advances in Physical Geochemistry. Springer, New York, pp. 153–171.

Genge, M.J., Jones, A.P., Price, G.D., 1995. An infrared and Raman study of carbonate glasses: implications for the structure of carbonatite magmas. Geochim. Cosmochim. Acta 59, 927–937. http://dx.doi.org/10.1016/0016-7037(95)00010-0.

Gudfinnsson, G.H., Presnall, D.C., 2005. Continuous gradations among primary carbonatitic, kimberlitic, melilititic, basaltic, picritic, and komatiitic melts in equilibrium with garnet lherzolite at 3–8 GPa. J. Petrol. 46, 1645–1659. http://dx.doi.org/10.1093/petrology/egi029.

Guillot, B., Sator, N., 2011. Carbon dioxide in silicate melts: a molecular dynamics simulation study. Geochim. Cosmochim. Acta 75, 1829–1857. http://dx.doi.org/10.1016/j.gca.2011.01.004.

Hiet, J., Deschamps, M., Pellerin, N., Fayon, F., Massiot, D., 2009. Probing chemical disorder in glasses using silicon-29 NMR spectral editing. Phys. Chem. Chem. Phys. 11, 6935–6940. http://dx.doi.org/10.1039/B906399D.

Holloway, J.R., Mysen, B.O., Eggler, D.H., 1976. The Solubility of CO_2 in Liquids on the Join CaO–MgO–SiO_2–CO_2. In: Carnegie Inst. Wash. Year Book, pp. 626–631.

Kohn, S.C., Brooker, R.A., Dupree, R., 1991. 13C MAS NMR: a method for studying CO_2 speciation in glasses. Geochim. Cosmochim. Acta 55, 3879–3884. http://dx.doi.org/10.1016/0016-7037(91)90082-G.

Konschak, A., 2008. CO_2 in Silikatschmelzen (Doctoral thesis). Bayreuth.

Konschak, A., Keppler, H., 2014. The speciation of carbon dioxide in silicate melts. Contrib. Mineral. Petrol. 167, 1–13. http://dx.doi.org/10.1007/s00410-014-0998-2.

Lee, S.K., Stebbins, J.F., 1999. The degree of aluminum avoidance in aluminosilicate glasses. Am. Mineral. 84, 937–945.

Lippmaa, E., Maegi, M., Samoson, A., Engelhardt, G., Grimmer, A.R., 1980. Structural studies of silicates by solid-state high-resolution silicon-29 NMR. J. Am. Chem. Soc. 102, 4889–4893. http://dx.doi.org/10.1021/ja00535a008.

Lippmaa, E., Maegi, M., Samoson, A., Tarmak, M., Engelhardt, G., 1981. Investigation of the structure of zeolites by solid-state high-resolution silicon-29 NMR spectroscopy. J. Am. Chem. Soc. 103, 4992–4996. http://dx.doi.org/10.1021/ja00407a002.

Maekawa, H., Maekawa, T., Kawamura, K., Yokokawa, T., 1991. The structural groups of alkali silicate glasses determined from ^{29}Si MAS-NMR. J. Non-Cryst. Solids 127, 53–64. http://dx.doi.org/10.1016/0022-3093(91)90400-Z.

Magi, M., Lippmaa, E., Samoson, A., Engelhardt, G., Grimmer, A.R., 1984. Solid-state high-resolution silicon-29 chemical shifts in silicates. J. Phys. Chem. 88, 1518–1522. http://dx.doi.org/10.1021/j150652a015.

Massiot, D., Messinger, R.J., Cadars, S., Deschamps, M., Montouillout, V., Pellerin, N., Veron, E., Allix, M., Florian, P., Fayon, F., 2013. Topological, geometric, and chemical order in materials: insights from solid-state NMR. Acc. Chem. Res. 46, 1975–1984. http://dx.doi.org/10.1021/ar3003255.

Massuyeau, M., Gardés, E., Morizet, Y., Gaillard, F., in press. A model for the activity of silica along the carbonatite–kimberlite–melilitite–basanite melt compositional joint. Chem. Geol. http://dx.doi.org/10.1016/j.chemgeo.2015.07.025, in press.

Morizet, Y., Kohn, S.C., Brooker, R.A., 2001. Annealing experiments on CO_2-bearing jadeite glass: an insight into the true temperature dependence of CO_2 speciation in silicate melts. Mineral. Mag. 65, 701–707. http://dx.doi.org/10.1180/0026461016560001.

Morizet, Y., Brooker, R.A., Kohn, S.C., 2002. CO_2 in haplo-phonolite melt: solubility, speciation and carbonate complexation. Geochim. Cosmochim. Acta 66, 1809–1820. http://dx.doi.org/10.1016/S0016-7037(01)00893-6.

Morizet, Y., Paris, M., Gaillard, F., Scaillet, B., 2014a. Carbon dioxide in silica-undersaturated melt. Part II: effect of CO_2 on quenched glass structure. Geochim. Cosmochim. Acta 144, 202–216. http://dx.doi.org/10.1016/j.gca.2014.08.034.

Morizet, Y., Paris, M., Gaillard, F., Scaillet, B., 2014b. Carbon dioxide in silica-undersaturated melt. Part I: the effect of mixed alkalis (K and Na) on CO_2 solubility and speciation. Geochim. Cosmochim. Acta 141, 45–61. http://dx.doi.org/10.1016/j.gca.2014.06.014.

Morizet, Y., Vuilleumier, R., Paris, M., 2015. A NMR and molecular dynamics study of CO_2-bearing basaltic melts and glasses. Chem. Geol. http://dx.doi.org/10.1016/j.chemgeo.2015.03.021.

Moussallam, Y., Morizet, Y., Massuyeau, M., Laumonier, M., Gaillard, F., 2014. CO_2 solubility in kimberlite melts. Chem. Geol. http://dx.doi.org/10.1016/j.chemgeo.2014.11.017.

Mysen, B.O., 1990. Effect of pressure, temperature, and bulk composition on the structure and species distribution in depolymerized alkali aluminosilicate melts and quenched melts. J. Geophys. Res., Solid Earth 95, 15733–15744. http://dx.doi.org/10.1029/JB095iB10p15733.

Mysen, B.O., 2007. The solution behavior of H_2O in peralkaline aluminosilicate melts at high pressure with implications for properties of hydrous melts. Geochim. Cosmochim. Acta 71, 1820–1834. http://dx.doi.org/10.1016/j.gca.2007.01.007.

Mysen, B.O., 2012. Lithos 148, 228–246. http://dx.doi.org/10.1016/j.lithos.2012.06.005.

Mysen, B., 2013. Structure–property relationships of COHN-saturated silicate melt coexisting with COHN fluid: a review of in-situ, high-temperature, high-pressure experiments. In: 9th Silicate Melts Workshop. Chem. Geol. 346, 113–124. http://dx.doi.org/10.1016/j.chemgeo.2012.10.006.

Mysen, B.O., Cody, G.D., 2005. Solution mechanisms of H_2O in depolymerized peralkaline melts. Geochim. Cosmochim. Acta 69, 5557–5566. http://dx.doi.org/10.1016/j.gca.2005.07.020.

Mysen, B., Richet, P., 2005. Silicate Glasses and Melts, Properties and Structure, 1st edn. Elsevier Science, Amsterdam.

Mysen, B.O., Virgo, D., 1980a. Solubility mechanisms of carbon dioxide in silicate melts; a Raman spectroscopic study. Am. Mineral. 65, 885–899.

Mysen, B.O., Virgo, D., 1980b. The solubility behavior of CO_2 in melts on the join $NaAlSi_3O_8$–$CaAl_2Si_2O_8$–CO_2 at high pressures and temperatures; a Raman spectroscopic study. Am. Mineral. 65, 1166–1175.

Mysen, B.O., Virgo, D., Seifert, F.A., 1982. The structure of silicate melts; implications for chemical and physical properties of natural magma. Rev. Geophys. Space Phys. 20, 353–383. http://dx.doi.org/10.1029/RG020i003p00353.

Nebel, H., Neumann, M., Mayer, C., Epple, M., 2008. On the structure of amorphous calcium carbonate—a detailed study by solid-state NMR spectroscopy. Inorg. Chem. 47, 7874–7879. http://dx.doi.org/10.1021/ic8007409.

Ni, H., Keppler, H., 2013. Carbon in silicate melts. Rev. Mineral. Geochem. 75, 251–287. http://dx.doi.org/10.2138/rmg.2013.75.9.

Nowak, M., Porbatzki, D., Spickenbom, K., Diedrich, O., 2003. Carbon dioxide speciation in silicate melts: a restart. Earth Planet. Sci. Lett. 207, 131–139. http://dx.doi.org/10.1016/S0012-821X(02)01145-7.

Papenguth, H.W., Kirkpatrick, R.J., Montez, B., Sandberg, P.A., 1989. ^{13}C MAS NMR spectroscopy of inorganic and biogenic carbonates. Am. Mineral. 74, 1152–1158.

Peccerillo, A., Poli, G., Serri, G., 1988. Petrogenesis of orenditic and kamafugitic rocks from central Italy. Can. Mineral. 26, 45–65.

Pommier, A., Evans, R.L., Key, K., Tyburczy, J.A., Mackwell, S., Elsenbeck, J., 2013. Prediction of silicate melt viscosity from electrical conductivity: a model and its geophysical implications. Geochem. Geophys. Geosyst. 14, 1685–1692. http://dx.doi.org/10.1002/ggge.20103.

Ragone, S.E., Datta, R.K., Roy, D.M., Tuttle, O.F., 1966. The system potassium carbonate—magnesium carbonate. J. Phys. Chem. 70, 3360–3361.

Sakamaki, T., Suzuki, A., Ohtani, E., Terasaki, H., Urakawa, S., Katayama, Y., Funakoshi, K., Wang, Y., Hernlund, J.W., Ballmer, M.D., 2013. Ponded melt at the boundary between the lithosphere and asthenosphere. Nat. Geosci. 6, 1041–1044. http://dx.doi.org/10.1038/ngeo1982.

Sakamaki, T., Kono, Y., Wang, Y., Park, C., Yu, T., Jing, Z., Shen, G., 2014. Contrasting sound velocity and intermediate-range structural order between polymerized and depolymerized silicate glasses under pressure. Earth Planet. Sci. Lett. 391, 288–295. http://dx.doi.org/10.1016/j.epsl.2014.02.008.

Schmerr, N., 2012. The gutenberg discontinuity: melt at the lithosphere–asthenosphere boundary. Science 335, 1480–1483. http://dx.doi.org/10.1126/science.1215433.

Schmidt, B.C., Riemer, T., Kohn, S.C., Behrens, H., Dupree, R., 2000. Different water solubility mechanisms in hydrous glasses along the Qz–Ab join: evidence from NMR spectroscopy. Geochim. Cosmochim. Acta 64, 513–526. http://dx.doi.org/10.1016/S0016-7037(99)00331-2.

Sharma, S.K., 1979. Structure and solubility of carbon dioxide in silicate glasses of diopside and sodium melilite compositions at high pressures from Raman spectroscopic data. In: Yearbook Carnegie Inst. Wash., pp. 532–537.

Sharma, S.K., Simons, B., 1980. Raman study of K_2CO_3 $MgCO_3$ glasses. In: Carnegie Inst. Wash Yearbook, vol. 79, pp. 322–326.

Sifre, D., Gardés, E., Massuyeau, M., Hashim, L., Hier-Majumder, S., Gaillard, F., 2014. The electrical conductivity during incipient melting in the oceanic low velocity zone. Nature.

Tinker, D., Lesher, C.E., Baxter, G.M., Uchida, T., Wang, Y., 2004. High-pressure viscometry of polymerized silicate melts and limitations of the Eyring equation. Am. Mineral. 89, 1701–1708.

Verweij, H., Van Den Boom, H., Breemer, R.E., 1977. Raman scattering of carbonate ions dissolved in potassium silicate glasses. J. Am. Ceram. Soc. 60, 529–534. http://dx.doi.org/10.1111/j.1151-2916.1977.tb14099.x.

Vuilleumier, R., Seitsonen, A.P., Sator, N., Guillot, B., 2015. Carbon dioxide in silicate melts at upper mantle conditions: insights from atomistic simulations. Chem. Geol. http://dx.doi.org/10.1016/j.chemgeo.2015.02.027.

White, W.B., 1974. The carbonate minerals. In: The Infrared Spectra of Minerals. In: Mineralogical Society of London Monograph, pp. 227–284.

Wyllie, P.J., 1989. Origin of Carbonatites; Evidence from Phase Equilibrium Studies. Unwin Hyman, London, United Kingdom, pp. 500–545.

Wyllie, P.J., Huang, W.-L., 1976. Carbonation and melting reactions in the system CaO–MgO–SiO_2–CO_2 at mantle pressures with geophysical and petrological applications. Contrib. Mineral. Petrol. 54, 79–107. http://dx.doi.org/10.1007/BF00372117.